Available online at www.sciencedirect.com
SCIENCE DIRECT®
Electrochimica Acta 51 (2005) 943–951
ELECTROCHIMICA Acta
www.elsevier.com/locate/electacta

Tin oxide nanosensor fabrication using AC dielectrophoretic manipulation of nanobelts

Surajit Kumar [a,*], Swaminathan Rajaraman [a], Rosario A. Gerhardt [b], Zhong Lin Wang [b], Peter J. Hesketh [a]

[a] *George W. Woodruff School of Mechanical Engineering, Georgia Institute of Technology, Room 321 Love Building, 771, Ferst Drive, Atlanta, GA 30332, USA*
[b] *School of Materials Science and Engineering, Georgia Institute of Technology, Atlanta, GA 30332, USA*

Received 20 October 2004; received in revised form 10 March 2005; accepted 15 April 2005
Available online 11 August 2005

Abstract

Nanobelts are a new class of semiconducting metal oxide nanowires. The ribbon-like nanobelts are chemically pure and structurally uniform single crystals, with clean, sharp, smooth surfaces, and rectangular cross-sections. Positive and negative dielectrophoresis (DEP) was demonstrated for the first time on semiconducting oxide nanobelts. This effect was then used for the fabrication of a nanodevice, which consisted of SnO_2 nanobelts attached to castellated gold electrodes defined on a glass substrate, and covered by a microchannel. The SnO_2 nanobelts (width ~ 100–300 nm, thickness ~ 30–40 nm) were suspended in ethanol and introduced into the microchannel. An alternating (AC) voltage of ~9.8 V peak to peak, with variable frequency, was applied between the electrodes (minimum electrode gap ~ 20 μm), which corresponds to an average electric field strength of less than 2.5×10^5 V/m. In the 10 Hz–1 kHz range, repulsion between the nanobelts and the electrodes occurred, while in the 1–10 MHz range, attraction was observed. Once the nanobelts touched the electrodes, those that were sufficiently long bridged the electrode gaps. The device was characterized and can potentially be used as a nanosensor.

Keywords: Nanobelt; Nanowire; AC dielectrophoresis; Nanosensor; SnO_2

1. Introduction

Dielectrophoresis (DEP) [1,2] is the force induced on a polarizable particle suspended in a fluid medium under the influence of non-uniform electric fields. In an electric field, a dielectric particle behaves as an effective dipole with induced dipole moment p, proportional to the electric field E [3], that is,

$$p \propto E \tag{1}$$

The constant of proportionality depends on the geometry of the dielectric particle. The force on a dipole, in the presence of electric field, is given by

$$F = (p \cdot \nabla)E \tag{2}$$

Combining the above two equations and using known results between p and E for a spherical particle, it has been shown that the dielectrophoresis force in an alternating (AC) field [1] is given by

$$F_{\mathrm{DEP}} = 2p\upsilon\varepsilon_{\mathrm{m}}\alpha_{\mathrm{r}}\nabla(E^2_{\mathrm{RMS}}) \tag{3}$$

where υ is the volume of the particle, ε_{m} the permittivity of the suspending medium, E_{RMS} the RMS value of the electric field, and a_{r} is the real part of the Claussius–Mossotti factor, $\mathrm{Re}[K(\omega)]$.

Homogeneous dielectric particles experience a Maxwell–Wagner interfacial polarization at a frequency determined by the relationship between the complex permittivities of the

* Corresponding author. Tel.: +1 404 385 2011; fax: +1 404 385 1417.
E-mail addresses: gtg916e@mail.gatech.edu, surajitk@yahoo.com (S. Kumar).

0013-4686/$ – see front matter © 2005 Elsevier Ltd. All rights reserved.
doi:10.1016/j.electacta.2005.04.068

particle and the surrounding medium, which is expressed by the real part of the Claussius–Mossotti factor,

$$\mathrm{Re}[K(\omega)] = \alpha_r = \mathrm{Re}\left(\frac{\varepsilon_p^* - \varepsilon_m^*}{\varepsilon_p^* + 2\varepsilon_m^*}\right) \quad (4)$$

where ε_m^* and ε_p^* are the complex permittivities of the medium and particle, respectively. The general complex permittivity is given by $\varepsilon^* = \varepsilon - j\sigma/\omega$, where ω is the angular frequency of the applied field, ε the permittivity, and σ is the conductivity. The surface conductivity is also included in the σ term [3]. Re[$K(\omega)$] is frequency dependent and determines both the magnitude and the sign of the dielectrophoretic force. The value of the a_r factor ranges from −0.5 to +1.0, and can be calculated from the properties of the medium and the particle. If the value of a_r is positive, the particle moves toward higher electric field regions, and is termed positive dielectrophoresis. If the value of a_r is negative, the particle moves toward lower electric field regions, and is termed negative dielectrophoresis. For a solid homogeneous particle undergoing a single interfacial relaxation process, the characteristic frequency at which the direction of the DEP force alternates is known as the crossover frequency. Analysis of the crossover frequency as a function of medium conductivity can be used to characterize the dielectric properties of a particle. This is at present the principal method of dielectrophoretic analysis of sub-micrometer particles such as latex beads [4,5] and viruses [6–8].

It has to be noted that Eq. (3) is a classical calculation on bulk material. Hence, it may not be quantitatively accurate for nanostructures and molecules. Surface charge and quantum effects are likely to affect the quantitative predictions [3]. However, the equation does give an idea of the variables involved and the possible trends.

Another effect of AC electric fields on polarizable objects is to orient them with respect to an electric field. The induced dipole moment p of the object interacts with the electric field to produce a torque T, given by [3]

$$T = p \times E \quad (5)$$

This effect is responsible for the alignment of DNA, nanotubes, nanowires, nanobelts, and such thin, long objects in fluid medium [3].

The DEP effect is independent of the charge on the particle [1]. Neutral particles are subject to this effect, and therefore DEP is more versatile in its applications for manipulating live cells, macromolecules, nanostructures, etc. Dielectrophoresis has traditionally been used for manipulating cells and other objects on the micrometer range (1–1000 μm) [1,2]. Only recently has it been used to study, manipulate, and separate nanometer scale objects such as latex spheres [4,5], viruses [6–8], nanowires [9], carbon nanotubes [10–13], and macromolecules [14,15].

AC dielectrophoretic alignment and assembly of metallic (Au) nanowires (35–350 nm diameter and up to 8 μm long) was demonstrated [16] by using a combination of floating and electrically contacted electrodes, field strengths of up to 10^7 V/m, and frequencies from 20 Hz to 20 kHz. Positive trapping of the Au nanowires was found at the floating electrodes for frequencies above 200 Hz, with the effectiveness increasing with higher frequencies. Iso-propyl alcohol (IPA) was the dielectric medium during the DEP assembly process.

Yamamoto et al. [11] performed dielectrophoresis studies on multi-walled carbon nanotubes (MWCNTs) of lengths between 1 μm and 5 μm, using Al electrodes with 400 μm gaps, field strengths of 2×10^5 V/m and iso-propyl alcohol as the dielectric medium. They observed alignment and attraction of the nanotubes to the electrodes (positive dielectrophoresis) for AC frequencies between 10 Hz and 10 MHz. The degree of alignment of the nanotubes increased with increasing frequency and increasing nanotube lengths. They also found that the alignment was more effective with AC dielectrophoresis compared to DC dielectrophoresis [12]. Similar studies were carried out on single walled carbon nanotubes (SWNTs) by Chen et al. [13]. The SWCNTs were dispersed in ethanol and electric field of 5×10^6 V/m intensity in the frequency range 500 Hz–5 MHz was applied. The DEP was positive for all frequencies studied. The SWCNTs were found to be oriented more strongly at higher frequencies. They found no effect of DC electric field on alignment.

A multi-walled carbon nanotube (MWCNT) based gas sensor fabricated using dielectrophoresis has been reported in the literature [17]. MWCNTs dispersed in ethanol were trapped and concentrated at an interdigitated microelectrode gap under the action of a positive DEP force. After the DEP process, the ethanol was evaporated and the microelectrode retaining the MWCNTs was exposed to ammonia (NH_3) gas. The electrode impedance was monitored and was found to change with ppm-levels of ammonia at room temperature. The ammonia exposure decreased the sensor conductance, while the capacitance increased. The conductance change was proportional to ammonia concentration below 10 ppm and then gradually saturated at higher concentrations.

To the best of our knowledge, the only reported dielectrophoresis work on semiconducting nanowires has been done by Duan et al. [9]. However, it was DC dielectrophoresis, which was used to align and electrically contact InP nanowires of 30 nm diameter to Ni/In/Au contact electrodes. The electrode gap separation was about 25 μm and the electric field strength between the electrodes was $\sim 10^7$ V/m. Chlorobenzene was used as the solvent medium, so that electrolysis was not an issue, since high DC voltages (100 V) were used in the dielectrophoresis process. They were able to align InP nanowires into a cross-bar topology using a layer-by-layer application of dielectrophoresis. AC dielectrophoresis on semiconducting material nanowires has not been reported so far.

An excellent review of the applications of dielectrophoresis in nanotechnology and future possibilities has been presented by Burke [3]. To use dielectrophoresis in pre-

cise alignment and placement of nano-objects for fabrication of nanodevices, a lot of work still needs to be done.

Nanobelts [18], which are a new class of semiconducting metal oxide nanowires (SnO_2, ZnO, In_2O_3, etc.), have been developed in our university (Georgia Institute of Technology). The ribbon-like nanobelts are chemically pure single crystals. They are structurally uniform with clean, sharp, smooth surfaces, and have rectangular cross-sections.

SnO_2 nanobelts can be used to make various types of sensors. Gas sensing has been demonstrated [19]. In this work, the nanobelts were simply dispersed onto a pre-patterned interdigitated planar electrode. Alignment was not performed. The principle of gas sensing is that the electrical conductivity of SnO_2 is sensitive to molecules adsorbed on its surface. Hence, monitoring the current or conductance through a nanobelt device allows the detection of gases. On exposure to CO, NO_2, and ethanol vapor on the sensor device at 400 °C, large changes in current were observed.

The possibility of using semiconducting nanowires for chemical and biological detection has also been demonstrated [20]. Boron-doped silicon nanowires (SiNWs) were used to create highly sensitive, real-time electrically based sensors for biological and chemical species. Changes in pH, streptavidin binding at picomolar concentrations, and antigen–antibody binding were detected in real time. The small size and capability of semiconductor nanowires are likely to be used in array-based screening and in vivo diagnostics for sensitive, label-free, real-time detection of a wide range of chemical and biological species [20].

Field effect transistors (FET) based on single semiconducting oxide nanobelts (ZnO and SnO_2) have been made [21]. Switching ratios of 6 orders of magnitude and high conductivities ($\sim 15\ \Omega^{-1}\ cm^{-1}$) were observed. The FET based on SnO_2 was also used as a gas sensor. Annealing the SnO_2 nanobelt FETs in an oxygen-deficient atmosphere produced a negative shift in the gate threshold voltage, which was explained as due to doping, induced by the generation of surface oxygen vacancies. This treatment can effectively tune the electrical performance of the nanobelt devices. The ZnO nanobelt FETs showed sensitivity to ultraviolet light, because of photogenerated electron–hole pairs and doping by UV induced surface desorption.

DEP devices have been developed using different fabrication techniques and electrode designs for different applications: traveling wave dielectrophoresis [22], insulating posts [23], manipulation of bioparticles and macromolecules [24], cell detection and manipulation [25,26], etc. In this paper, we present a rapid, low cost, in-house technique that can be used to fabricate DEP devices either on a research scale or for mass production for manipulating nanobelts/nanowires. Using such a device, positive and negative dielectrophoresis was demonstrated on semiconducting oxide nanobelts (SnO_2). Characterization experiments suggest that these nanodevices have potential to be used as nanosensors.

2. Experimental

The manipulation of nanobelts was carried out with DEP at an array of castellated microelectrodes deposited on Pyrex glass. The microelectrode array was covered with a microchannel so that the nanobelt suspension could be pumped into the stereolithographically (SLA) defined microchannel.

2.1. Fabrication of the microelectrodes

Fabrication of the electrodes was carried out on 1 mm thick Pyrex glass substrates (G.M. Associates Inc., Oakland, CA, USA). The transparent substrate allows visualization of the nanobelt manipulation from the bottom side using an inverted microscope. The substrates were cleaned to improve adhesion using a base clean solution (5:1:1 solution of DI/NH_4OH/H_2O_2), and then treated with O_2 plasma for 15 min in a RIE system (Plasma-Therm Inc.). The Ti/Au electrode was patterned on the wafer using standard lithographic techniques and lift-off process. First, the pattern was defined in negative acting NR5-8000 photoresist (Futurrex Inc., Franklin, NJ, USA). After treating the wafer with oxygen plasma for 3–5 min, a 300 Å thick titanium (Ti) layer and a 2500 Å thick gold (Au) layer were deposited using an electron beam evaporator system (CVC Products). The sample was dipped in acetone for about 10 min to remove the photoresist, making the electrodes ready for use.

The pattern of the electrodes is castellated in nature as shown in Fig. 1. The fabrication process flow is summarized in Fig. 2. The steps are: (a) start with glass substrate, (b) pattern formation after lithography, (c) metal (Ti/Au) deposition, (d) lift-off using acetone, and finally, (e) covering the electrodes with SLA microchannel.

2.2. Fabrication of the SLA microchannel

Stereolithography is a rapid prototyping technique [27,28] that can be used for making parts of complicated geometry. The advantages of SLA process are the rapid fabrication and design flexibility. The microchannel, with a channel depth of about 150 μm, has an inlet and an outlet (see Fig. 3(a and b)) so that the nanobelt suspension could be pumped through.

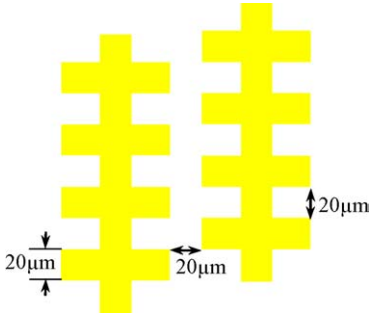

Fig. 1. Castellated structure of the DEP microelectrodes.

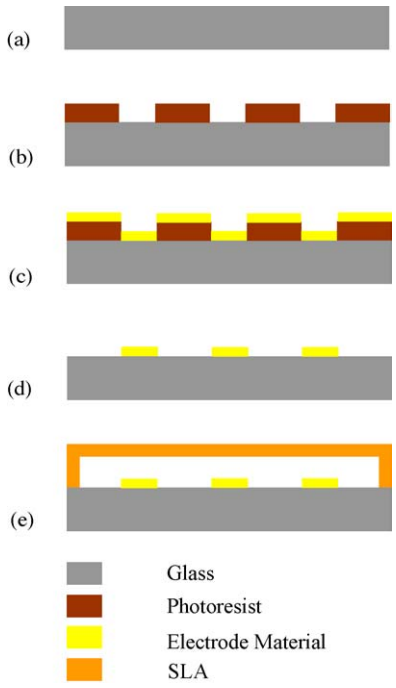

Fig. 2. Schematic diagram of process flow (steps (a–e)) used in the fabrication of the DEP device.

The SLA microchannel fabrication was performed using a 3D Systems Viper 1500 (3D Systems Corporation, Valencia, CA, USA) machine. Stereolithography resin Vantico SL 5510 (Huntsman Advanced Materials, Salt Lake City, UT, USA) was used. The fabrication process involves the curing of the resin layer by layer using a computer controlled laser. The fabricated parts are then cleaned in iso-propyl alcohol and cured in an ultraviolet (UV) oven for 90 min.

2.3. Assembly of the microelectrodes and the SLA part

The SLA microchannel and Pyrex substrate were carefully aligned and bonded with epoxy (Loctite Extra Time, Henkel Consumer Adhesives, Avon, OH, USA) to assemble the DEP device. Electrical connections were made using gold wires and conductive epoxy (Loctite 3880, Henkel Consumer Adhesives). A layer of epoxy (Loctite Extra Time) was then coated on the wire bonds to prevent them from breaking off. Fig. 3(a and b) shows the assembled DEP device. The width and length of the SLA microchannel are 1 cm and 2 cm, respectively. Two different electrode connections were established. They are marked as E1 and E2 in Fig. 3(a).

2.4. SnO_2 nanobelt sample

SnO_2 nanobelt samples were made using the thermal evaporation method outlined in [18,29,30]. It is a process in which condensed powder source material is vaporized at an elevated temperature in a tube furnace and the resultant vapor is condensed under controlled conditions (temperature, pressure, atmosphere, substrate, etc.) to form the desired product. Argon (Ar) carrier gas enters the alumina tube in the furnace (50 cm long, 4 cm diameter), and is pumped out by the rotary pump. The source material is loaded on an alumina boat and positioned at the center of the tube. Several alumina plates (60 mm × 10 mm) were placed downstream, one behind the other, inside the alumina tube, which acted as substrates for collecting growth products. At a pressure of 200–600 Torr, thermal evaporation of SnO powder (purity 99.9%, melting point 1080 °C) was carried out at ∼1050 °C for 2 h, under an Ar carrier gas flow of 50 sccm. The substrate temperature was carefully controlled during the deposition. The same nanostructure can also be made at 1350 °C from SnO_2 powder (purity 99.9%, melting point 1630 °C) [29,30].

The nanobelt product obtained from the furnace is in the form of agglomerates, with the individual nanobelts intertwined with one another. The individual nanobelts can be very long (∼500 μm). In order to use the nanobelts in a device, it is necessary to separate the agglomerates into individual nanobelts. Hence, ultra-sonication of the nanobelt agglomerate was carried out in ethanol.

Fig. 4 shows an image of SnO_2 nanobelts dispersed on Au/Si substrate (gold layer on top of silicon). The ethanol was evaporated and the sample observed under an optical microscope. The length distribution of the nanobelts depends

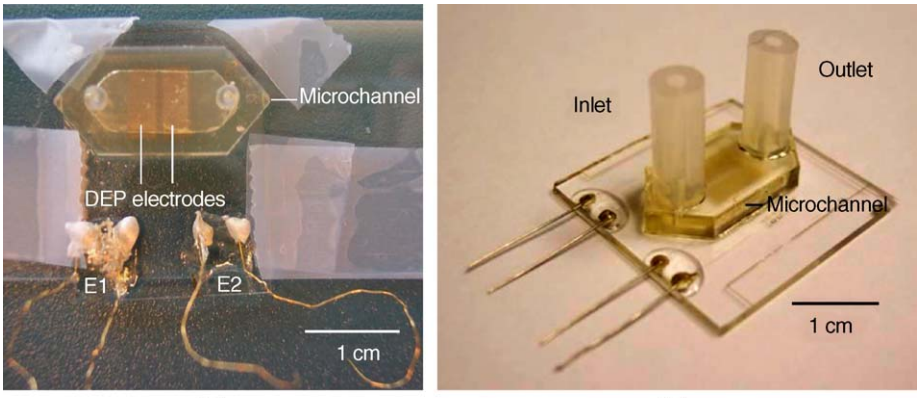

(a) (b)

Fig. 3. Assembled DEP device: (a) top view showing the electrodes under the SLA microchannel and (b) view at an angle showing the fluidic connections.

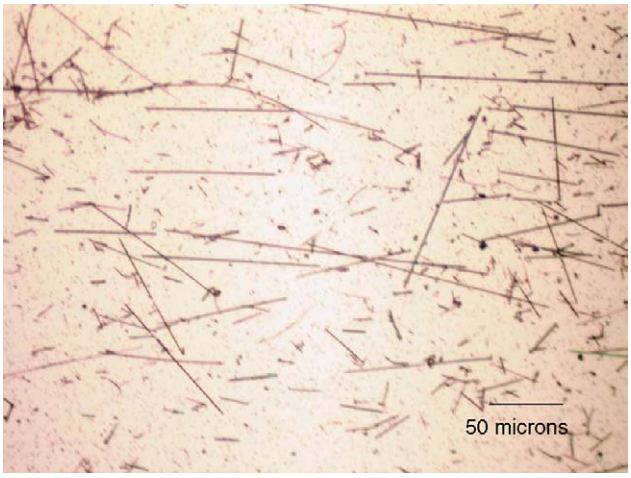

Fig. 4. Optical microscope image of SnO_2 nanobelts dispersed on Au/Si substrate. The lengths of the nanobelts vary depending on the sonication time.

on the sonication time used to break up the initially long nanobelts. In the photograph, both short and long nanobelts are visible. The nanobelts used in the tests had a width in the range of 100–300 nm, so that it could be observed under an optical microscope as a dark line. Typical atomic force microscope (AFM) measurements indicate that the nanobelts are 30–40 nm thick. Separate SEM measurements on the nanobelt samples used in the DEP device have also confirmed that the thickness is in that range. The size range is determined by the growth conditions [18,29,30].

2.5. Experimental setup and testing

Flexible Tygon tubings of 1.02 mm ID were attached to the inlet and outlet of the DEP device. A 20 ml syringe was filled with the nanobelt suspension and used with a syringe pump to pump the nanobelt suspension through the DEP system at a controlled flow rate (0.05–0.10 ml/min). Once the suspension started flowing, an AC voltage of 9.8 V peak to peak was applied between the electrodes using a Synthesized Function Generator (Stanford Research Systems Inc., Sunnyvale, CA, USA). Frequency was varied from 10 Hz to 10 MHz and the effect on the nanobelts was observed. During the experiment, the flow time was monitored so that the number of nanobelts bridging the electrode gaps could be controlled. The nanobelts could be seen as dark lines through the Nikon Eclipse TE2000-S (Nikon Instruments Inc., Melville, NY, USA) inverted microscope. Digital images were taken using a computer controlled imaging software, MetaMorph® Imaging System (Universal Imaging Corporation, Downingtown, PA, USA), which enabled automated image capture and analysis from a digital CCD camera attached to the microscope.

After the dielectrophoresis experiment, the ethanol in the device was dried. Application of DC voltage between the electrodes caused current to flow through the nanobelts between the electrodes. It was apparent that electrical contact between the gold electrodes and the SnO_2 nanobelts had taken place. Various tests were performed using the DEP device to characterize it, which involved measurements of current, voltage, and impedance. The effect of changes in temperature and lighting conditions was also studied.

LabVIEW software (National Instruments Corporation, Austin, TX, USA) was used for data acquisition. For current and voltage measurements, a Keithley 195A Digital Multimeter (Keithley Instruments Inc., Cleveland, OH, USA) was used in combination with Tektronix PS2520G Programmable Power Supply (Tektronix Inc., Beaverton, OR, USA). The LabVIEW software could also scan the applied voltage at a predetermined scan rate and record the current.

As a source of visible light, a Model 180-Standard 150 W Illuminator (Dolan-Jenner Industries Inc., Lawrence, MA, USA) with a quartz halogen lamp was used. For UV light, a Blak-Ray Model B-100A (Blak-Ray Inc., San Gabriel, CA, USA), which emits UV radiation at 365 nm wavelength, was used.

For impedance measurements, Solartron SI 1260 Impedance/Gain-Phase Analyzer (Solartron Analytical, England) was used in combination with Solartron 1296 Dielectric Interface. The range of the frequency sweep was 0.01 Hz–10 MHz.

Measurements were performed in ambient under different lighting conditions—no light, visible light, and UV light exposures. The effect of temperature was studied under inert conditions, by flowing dry nitrogen through the DEP microchannel, while an electrical strip heater was attached to the Pyrex glass (bottom of the DEP device). A variable DC current source was attached to the heater to control the temperature of the device.

3. Results and discussion

3.1. Dielectrophoresis

Fig. 5 shows the DEP electrodes as observed under the inverted microscope. The electric field is between the alter-

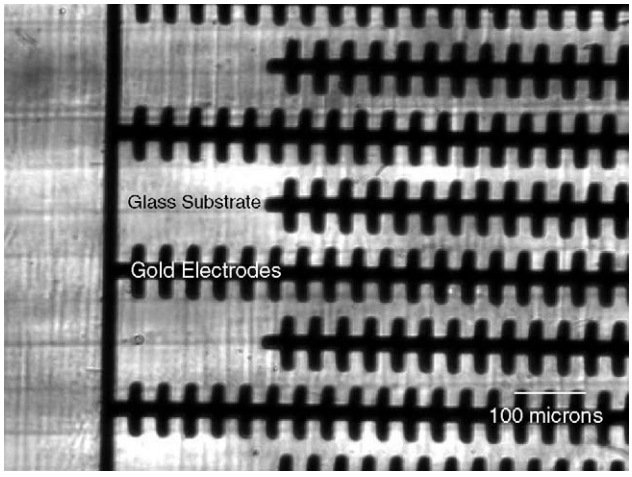

Fig. 5. An optical microscope photograph of the DEP electrodes, showing their structure. The electric field is between the alternating branches.

nating branches. As explained in Section 2, the SnO_2 nanobelt suspension was introduced into the microchannel and manipulated using AC voltages with different frequencies. The voltage applied was 9.8 V peak to peak. This corresponds to an average electric field of $\sim 2.5 \times 10^5$ V/m between the electrodes, which is quite low compared to other dielectrophoresis studies [9,16]. It was observed that in the 10 Hz–1 kHz (low) frequency range, repulsion of the nanobelts from the electrodes occurred, which demonstrates negative dielectrophoresis. The nanobelts were seen vibrating in the gaps between the electrodes such that the ends of the nanobelts were away from the electrodes (aligned perpendicular to a line connecting the gaps). In the 1–10 MHz (high) frequency range, the nanobelts were attracted between the electrodes (positive dielectrophoresis). The reason for the alignment under low electric field (2.5×10^5 V/m) is possibly the long length of the nanobelts (see Fig. 4). In a similar study on carbon nanotubes (MWNTs) [11], it was found that longer nanotubes were attracted and aligned more easily than shorter ones.

Attraction of the nanobelts between the electrodes caused the nanobelts to touch the electrodes. Once the nanobelts made contact with the electrodes, they remained stuck there. The dielectrophoretic effect was lost, since the nanobelts were bridging the gap. Fig. 6 shows the situation during positive dielectrophoresis. The longer nanobelts bridged the electrode gaps and were not affected further by the AC voltage. However, the short nanobelts which could not bridge the electrode gaps are seen to be sticking out in the direction of the maximum field gradient. As flow of the suspension continued, the number of nanobelts between the gaps increased with time. This was verified later from the *i–V* characteristics of the devices. Devices in which more flow time was allowed showed higher current levels. It was also observed that if the flow was stopped, the manipulation was still possible, since the fluid (ethanol) was inside the microchannel, suspending the nanobelts. In fact, that provides insight into a possible way of making nanodevices. Microelectrodes can be fabricated and a drop of nanobelt suspension applied on the electrodes. Application of AC voltage will allow the nanobelts to make contacts with the electrodes.

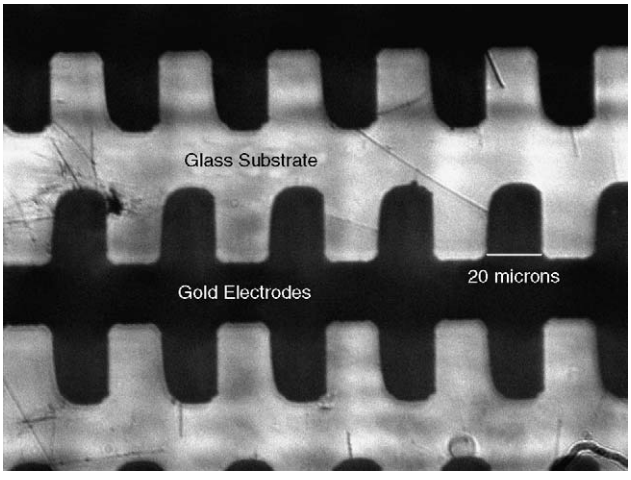

Fig. 6. SnO_2 nanobelts bridging DEP electrode gaps during positive dielectrophoresis. Smaller nanobelts are sticking out of the electrodes due to the action of the electric field.

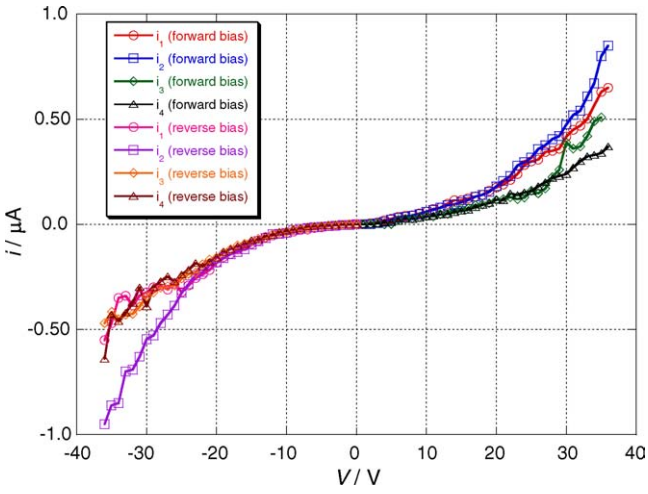

Fig. 7. *i–V* characteristics of SnO_2 nanobelts bridging the dielectrophoretic electrode gaps (electrode pair E1).

3.2. *i–V curves*

In the DEP device, there were two sets of dielectrophoretic electrodes E1 and E2 (see Fig. 3(a)). Voltage could be applied independently to each of them, although both are inside the same microchannel. In one of the electrode pairs (E1), the number of trapped nanobelts is smaller than in the other electrode pair (E2). We can deduce this fact because the current levels in the *i–V* curves is orders of magnitude different for each electrode pair. This is also confirmed from the impedance measurements. Figs. 7 and 8 show *i–V* curves for DEP electrode pairs E1 and E2, respectively. The *i–V* charac-

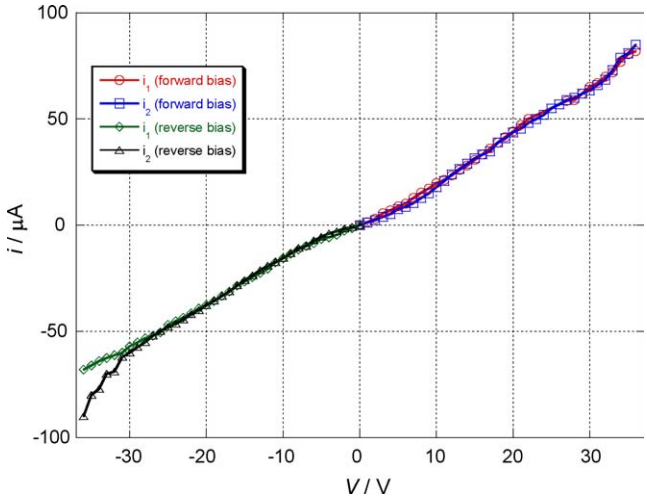

Fig. 8. *i–V* characteristics of SnO_2 nanobelts bridging the dielectrophoretic electrode gaps (electrode pair E2).

teristics are very different in the two cases. In the case of E1, the curves are non-linear and close to exponential, indicating non-ohmic contacts, which is characteristic of metal (Au), semiconductor (SnO_2) junction. However, the *i–V* curves for E2 are close to linear. A possible explanation for this behavior is that because of the varying levels of contact of the large numbers of nanobelts involved in E2, the non-ohmic behavior of the individual nanobelts averages out and gives an almost linear curve. Forward and reverse bias characteristics are similar in both cases.

3.3. Effect of temperature

The effect of temperature on the nanobelt device was studied in an inert dry nitrogen atmosphere. The heater current is representative of the temperature in the electrodes. Fig. 9 shows a plot demonstrating the effect of temperature on the current through the nanobelt device (electrode pair E1) at a bias of 10 V DC. Please note the log scale in the plot. The current through the device increased as the current in the strip heater was raised. The current in the device changed from a low level steady-state value, sharply to reach the high level steady-state value, showing that the temperature of the device and hence the nanobelts were changing during the transient period. The semiconducting behavior of the nanobelts is clear from this result. Current through the nanobelt increased exponentially with temperature. Log of the nanobelt steady-state current is proportional to the current in the strip heater used to heat the device, as indicated by the constant level changes in the device current (steady state) when the heater current is changed in magnitude two times and then three times.

3.4. Effect of visible and UV light exposure

Tests were performed to see the effect of visible and UV light on the current (conductivity) of the nanobelts under

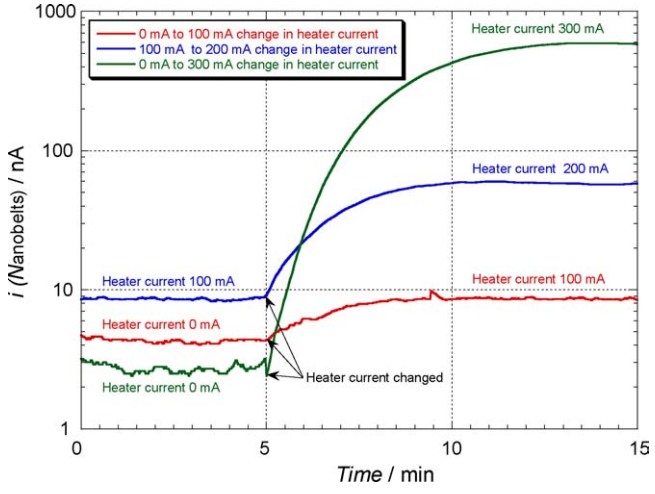

Fig. 9. Plot showing the effect of temperature on the current through the nanobelt device (electrode pair E1).

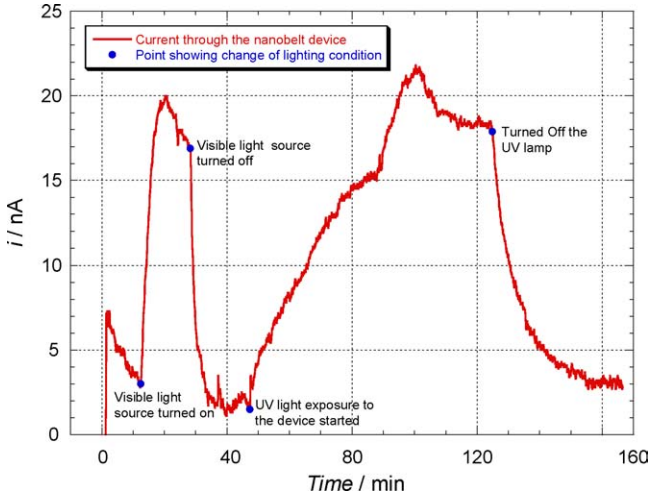

Fig. 10. Plot showing the effect of visible and UV light on the SnO_2 nanobelts between the gold electrodes (electrode pair E1) under a bias of 10 V DC.

atmospheric conditions. Fig. 10 is a plot of the current through the DEP device (electrode pair E1) as a function of time, with periodic visible light and UV light exposures. The response to visible light was faster than the response to the UV light. The increase in the conductivity due to UV light results from both photogeneration of electron–hole pairs as well as doping by UV light induced surface desorption of adsorbed molecules [31–33]. Since the light effect experiments were performed in open air (humidity), surface adsorption and desorption of various molecules (e.g., O_2, H_2O, etc.) are possible. The slow response is most probably due to that effect. Further investigation is ongoing to examine UV light sensitivity under controlled ambient conditions. In additions, studies are being done to find out the reason for the visible light response of the SnO_2 nanobelts.

Impedance measurements have also demonstrated the effect of light clearly. The impedance decreases when the SnO_2 nanobelts are exposed to visible and UV light. Those results are presented in the next section.

3.5. Impedance measurements

Impedance measurements were performed on the SnO_2 nanobelts with different lighting conditions. Fig. 11 shows impedance as a function of frequency (Bode plots) for the E2 electrode pair. The effect of light is clearly demonstrated. The curve with the highest impedance corresponds to the no light case. Exposure of visible light of low intensity decreased the impedance. Increasing the intensity of the visible light caused further decrease in the impedance. UV light also caused a decreased in the impedance. Please note that the intensity of the visible light and the UV light are not necessarily the same. The flat portion of the Bode plot in low frequency range indicates the value of the resistance of the sample under study. It is clear that application of light

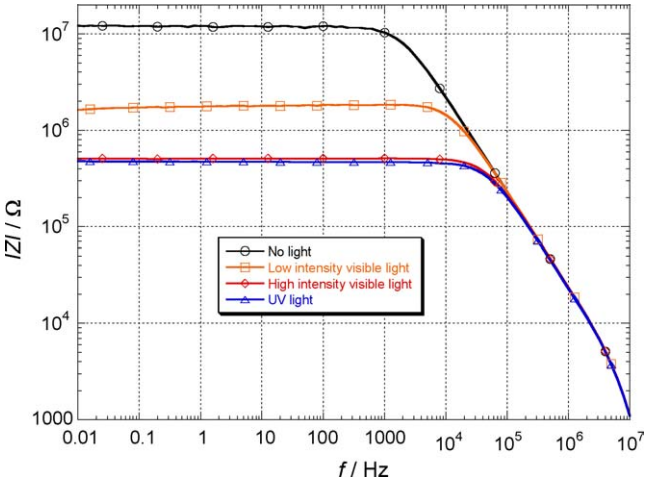

Fig. 11. Bode plot showing frequency response of the impedance of SnO_2 nanobelts in the DEP device (electrode pair E2).

causes an order of magnitude decrease in resistance of the device.

Complex impedance plots are shown in Fig. 12 for the E2 electrode pair. The complex impedance plots show a single semi-circle in each case, which implies resistance–capacitance parallel equivalent circuit. The decreasing radii of the semi-circles in the complex impedance plot demonstrates the decrease in resistance of the device upon the application of light.

3.6. Conclusions and future work

For the first time, we have demonstrated positive and negative dielectrophoresis on semiconducting material based nanobelt/nanowires using AC electric fields. 9.8 V peak to peak AC was used between the DEP electrodes (20 μm electrode gap) with variable frequency. This corresponds to an average electric field of $\sim 2.5 \times 10^5$ V/m, which is quite low compared to other dielectrophoresis studies [9,16] on nanowires. However, it has to be kept in mind that there is a variation of electric field between the electrode gaps. In the low frequency range (10 Hz–1 kHz) negative dielectrophoresis occurred, while in the high frequency range (1–10 MHz) positive dielectrophoresis was observed. We have not attempted to produce electrodes with less than 10 μm gap although smaller gaps have been reported in the literature [34]. With smaller electrode gaps, lower voltages are expected for the dielectrophoretic manipulation.

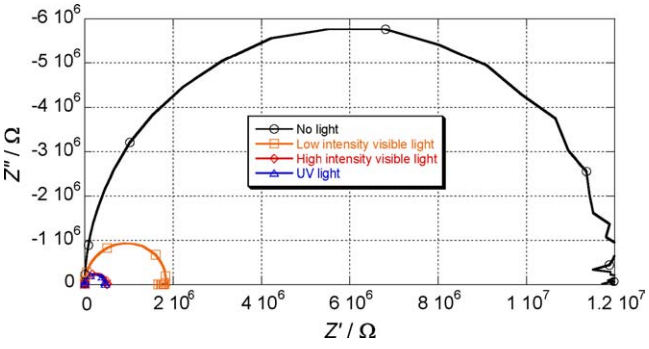

Fig. 12. Complex impedance plot of the SnO_2 nanobelts in the DEP device (electrode E2). The frequency increases counter-clockwise on the semi-circles.

The dielectrophoretic manipulation of the SnO_2 nanobelts resulted in a nanodevice. Several characterization methods were used to study it. The effect of temperature and light on conductivity of the SnO_2 nanobelt device was studied and shown to demonstrate substantial effects. Use of the device as a gas sensor is currently being investigated. Since SnO_2 nanobelt conductivity is sensitive to gases adsorbed on its surface [19], it is very likely that the present device can be used as a gas sensor. The effect of light exposure is being further investigated to use the nanobelt as a light sensor.

More studies can be undertaken to understand the dielectric characteristics of SnO_2 nanobelts. Analysis of the crossover frequency [4,5] as a function of medium conductivity can possibly be used to characterize them. The influence of the surface conductance of the nano-object may also be an important factor in the dielectrophoresis of semiconducting oxide materials.

Other techniques such as traveling wave dielectrophoresis [22], electrorotation [35], etc., will be found useful in nanomanipulation of semiconductor based nanowires/nanobelts in addition to the AC dielectrophoresis that has been demonstrated in the present work. Building single nanobelt/nanowire devices will require improved electrode design to obtain optimum field distribution and better manipulation. In addition, control of the concentration of the nano-object in the suspension fluid (so that fewer number of nano-objects come under the electric field of the electrodes) and a study of the dielectric properties of the nano-object and the suspension fluid as a function of frequency (so that the positive and negative DEP regions can be determined) will be found useful in achieving that goal.

Acknowledgements

The authors wish to acknowledge the financial support of Nanoscience and Nanotechnology Fellowship Committee of Georgia Institute of Technology for funding through a NaST Fellowship to the first author. The second author was supported by the Homeland Security Initiative at Georgia Tech Research Institute, which is appreciated. The authors would also like to acknowledge the efforts of Arnab Choudhury, Jeff Street, and Dr. Chi-Fu Wu in fabrication of the stereolithography parts, and the staff of Microelectronics Research Center (MiRC) at Georgia Tech for the clean room facilities used for the work. Special thanks go to Dr. Xiangyang Kong for making the nanobelt sample, Daren Whitelock for writing LabVIEW programs for data acquisition, and Dr. Runqing Ou for helping with some of the electrical measurements.

References

[1] H.A. Pohl, Dielectrophoresis, Cambridge University Press, Cambridge, 1978.
[2] T.B. Jones, Electromechanics of Particles, Cambridge University Press, Cambridge, 1995.
[3] P.J. Burke, in: H.S. Nalwa (Ed.), Encyclopedia of Nanoscience and Nanotechnology, vol. 10, American Scientific Publishers, Stevenson Ranch, CA, 2003, pp. 1–19.
[4] M.P. Hughes, J. Colloid Interface Sci. 250 (2) (2002) 291.
[5] M.P. Hughes, H. Morgan, M.F. Flynn, J. Colloid Interface Sci. 220 (2) (1999) 454.
[6] M.P. Hughes, H. Morgan, F.J. Rixon, J.P.H. Burt, R. Pethig, Biochim. Biophys. Acta 1425 (1998) 119.
[7] M.P. Hughes, H. Morgan, F.J. Rixon, Eur. Biophys. J. 30 (1998) 268.
[8] N.G. Green, H. Morgan, J.J. Milner, Biochem. Biophys. Methods 35 (1997) 89.
[9] X. Duan, Y. Huang, Y. Cui, J. Wang, C.M. Lieber, Nature 409 (2001) 66.
[10] R. Krupke, F. Hennrich, H. von Lohneysen, M.M. Kappes, Science 301 (5631) (2003) 344.
[11] K. Yamamoto, S. Akita, Y. Nakayama, J. Phys. D 31 (1998) L34.
[12] K. Yamamoto, S. Akita, Y. Nakayama, Jpn. J. Appl. Phys. 2, 35 (7B) (1996) L917.
[13] X.Q. Chen, T. Saito, H. Yamada, K. Matsushige, Appl. Phys. Lett. 78 (2001) 3714.
[14] M. Washizu, S. Suzuki, O. Kurosawa, T. Nishizaka, T. Shinohara, IEEE Trans. Ind. Appl. 30 (1994) 835.
[15] D. Porath, A. Bezryadin, S. de Vries, C. Dekker, Nature 403 (2000) 635.
[16] P.A. Smith, C.D. Nordquist, T.N. Jackson, T.S. Mayer, B.R. Martin, J. Mbindyo, T.E. Mallouk, Appl. Phys. Lett. 77 (9) (2000) 1399.
[17] J. Suehiro, G. Zhou, M. Hara, J. Phys. D: Appl. Phys. 36 (2003) L109.
[18] Z.W. Pan, Z.R. Dai, Z.L. Wang, Science 291 (2001) 1947.
[19] E. Comini, G. Faglia, G. Sberveglieria, Z. Pan, Z.L. Wang, Appl. Phys. Lett. 81 (10) (2002) 1869.
[20] Y. Cui, Q. Wei, H. Park, C.M. Lieber, Science 293 (5533) (2001) 1289.
[21] M. Arnold, P. Avouris, Z.W. Pan, Z.L. Wang, J. Phys. Chem. B 107 (2003) 659.
[22] L. Cui, H. Morgan, J. Micromech. Microeng. 10 (2000) 72.
[23] E.B. Cummings, A.K. Singh, Anal. Chem. 75 (18) (2003) 4724.
[24] Y. Huang, K.L. Ewalt, M. Tirado, R. Haigis, A. Forster, D. Ackley, M.J. Heller, J.P. O'Connell, M. Krihak, Anal. Chem. 73 (7) (2001) 1549.
[25] G. Medero, N. Manaresi, A. Leonardi, L. Altomare, M. Tartagni, R. Guerrieri, IEEE Sens. J. 3 (2003) 317.
[26] H.B. Li, R. Bashir, Sens. Actuators B 86 (2002) 215.
[27] P.F. Jacobs, Stereolithography and Other RP&M Technologies: From Rapid Prototyping to Rapid Tooling, ASME Press, New York, NY, 1996.
[28] R. Pethig, Crit. Rev. Biotechnol. 16 (1996) 331.
[29] Z.R. Dai, Z.W. Pan, Z.L. Wang, Adv. Funct. Mater. 13 (2003) 9.
[30] Z.L. Wang, Adv. Mater. 15 (2003) 432.
[31] D.H. Zhang, Mater. Chem. Phys. 45 (1996) 248.
[32] P. Bonasewicz, W. Hirschwald, G. Neumann, J. Electrochem. Soc. 133 (1986) 2270.
[33] Y. Shapira, S.M. Cox, D. Lichtma, Surf. Sci. 54 (1976) 43.
[34] E. Forsén, P. Carlberg, L. Montelius, A. Boisen, Microelectron. Eng. 73–74 (2004) 491.
[35] M.P. Hughes, S. Archer, H. Morgan, J. Phys. D: Appl. Phys. 32 (13) (1999) 1548.